Journal of Colloid and Interface Science 650 (2023) 1393–1405

Contents lists available at ScienceDirect

Journal of Colloid And Interface Science

journal homepage: www.elsevier.com/locate/jcis

Probing ion-binding at a protein interface: Modulation of protein properties by ionic liquids

Qi Han [a], Yuyu Su [b], Kate M. Smith [c,d], Jack Binns [a], Calum J. Drummond [a,*], Connie Darmanin [e,*], Tamar L. Greaves [a,*]

[a] School of Science, STEM College, RMIT University, Melbourne, VIC 3000, Australia
[b] School of Engineering, STEM College, RMIT University, Melbourne, VIC 3000, Australia
[c] Australian Synchrotron, Australian Nuclear Science and Technology Organisation, 800 Blackburn Road, Clayton, VIC 3168, Australia
[d] Swiss Light Source, Paul Scherrer Institute, Forschungsstrasse 111, Villigen-PSI, 5232 Villigen, Switzerland
[e] La Trobe Institute for Molecular Science, Department of Mathematical and Physical Sciences, School of Computing Engineering and Mathematical Science, La Trobe University, Bundoora, VIC 3086, Australia

GRAPHICAL ABSTRACT

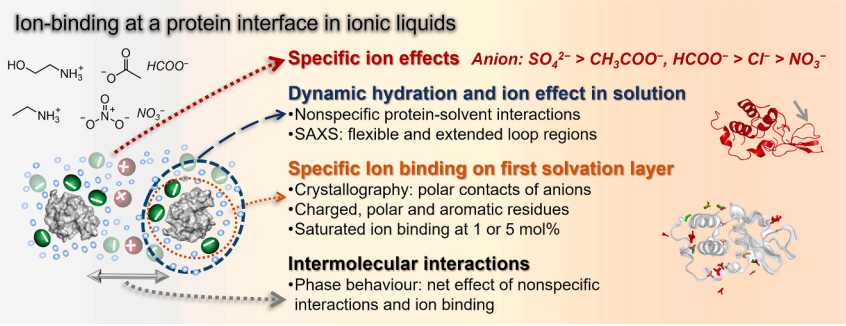

ARTICLE INFO

Keywords:
Protein-ion binding
Protein-solvent interaction
Protein interface
Specific ion effects
Ionic liquid
Protein aggregation
X-ray crystallography
Small-angle X-ray scattering
Lysozyme

ABSTRACT

Ions are important to modulate protein properties, including solubility and stability, through specific ion effects. Ionic liquids (ILs) are designer salts with versatile ion combinations with great potential to control protein properties. Although protein-ion binding of common metals is well-known, the IL effect on proteins is not well understood. Here, we employ the model protein lysozyme in dilute and concentrated IL solutions to determine the specific ion binding effect on protein phase behaviour, activity, size and conformational change, aggregation and intermolecular interactions. A combination of spectroscopic techniques, activity assays, small-angle X-ray scattering, and crystallography highlights that ILs, particularly their anions, bind to specific sites in the protein hydration layer via polar contacts on charged, polar and aromatic residues. The specific ion binding can induce more flexible loop regions in lysozyme, while the ion binding in the bulk phase can be more dynamic in solution. Overall, the protein behaviour in ILs depends on the net effect of nonspecific interactions and specific ion binding. Compared to formate, the nitrate anion induced high protein solubility, low activity, elongated shape

* Corresponding authors.
E-mail addresses: calum.drummond@rmit.edu.au (C.J. Drummond), c.darmanin@latrobe.edu.au (C. Darmanin), tamar.greaves@rmit.edu.au (T.L. Greaves).

https://doi.org/10.1016/j.jcis.2023.07.045
Received 25 April 2023; Received in revised form 5 July 2023; Accepted 8 July 2023
Available online 11 July 2023
0021-9797/© 2023 The Author(s). Published by Elsevier Inc. This is an open access article under the CC BY-NC license (http://creativecommons.org/licenses/by-nc/4.0/).

and aggregation, which is largely owing to its higher propensity for ion binding. These findings provide new insights into protein-IL binding interactions and using ILs to modulate protein properties.

1. Introduction

In nature, proteins are often faced with multiple stresses such as temperature, pH, solvents, molecular and ionic additives, and interfacial tension and elasticity. Since most proteins require solvents to maintain their structures, it is a common practice to modulate stresses using salt additives in water. Although salts (including self-buffering agents, ammonium sulphate and guanidinium chloride) are widely used to control protein solubility, stability and activity, the number of known ion types acting as stabilisers or modifiers is limited. Ionic liquids (ILs) are an alternative solvating media type to the common high-melting salts and volatile media like water. ILs are designer solvents comprised of ions which have low to negligible volatility, and highly tunable physiochemical properties through modification of the cation and anion structures [1–3]. Compared with common salts, ILs typically have weaker Coulombic interactions, but many form distinct hydrogen bonding interactions, particularly in protic ILs (PILs) where protons are transferred [4,5]. Furthermore, ILs can engage in hydrophobic interactions by incorporating ions with alkyl chains [6]. One notable advantage of many select ILs is their ability to mix with water in any ratio, significantly expanding the concentration range of possible ionic additives [7,8]. Hence, the high solubility in water, the relatively simple synthesis and the frequently benign precursors of PILs render them easily accessible and suitable for high-throughput screening of protein solvent formulations [2,9].

Using water as a co-solvent with ILs is a common approach, where both the IL and protein concentration can be largely diluted. Effects of ions are regularly interpreted by Hofmeister series, and specific ion or electrostatic screening effects [7,10–12]. These effects are, however, often empirical and treat each ion independently, despite the known importance of ion pairing [13]. To date, structure–property relationships for specific ion effects on protein stability and hence protein-ion interactions is still an active area of discussion [14,15].

Characterizing proteins and their interactions with ions is often problematic owing to signal interference, the small free energies of the interactions and the occurrence of protein aggregation [16,17]. Previous investigations using ILs mainly employed a range of spectroscopic techniques to identify protein structural changes and the folding/unfolding transition, with IL concentration and the anion and nano-heterogeneous structure of ILs as the main controlling factors [18–20]. Recently, solution-based small-angle X-ray scattering (SAXS) has emerged as a high-accuracy and high-throughput approach [21,22], and can characterize protein size, shape, structure, and aggregation in ILs [23–25]. For example, SAXS-based structural models show that aqueous ethylammonium nitrate (EAN) maintained lysozyme structure [26]. However, concentrated ILs led to distinct protein aggregation and conformational changes, even with different ion species and stabilizers [24,26,27]. Protein crystallography is the principal technique to determine protein structures, despite being a complicated, multiparametric and time-consuming process. The first protein crystallization investigation involving ILs utilized NaCl with EAN as precipitants for lysozyme [28]. Since then, several studies have used ILs as additives to control protein crystallization behaviour with high yields and reproducibility [29–32]. Surprisingly, few protein structures have been determined with ILs present [33]. Only our previous lysozyme structure (PDB 7JMU) reported that anions directly interacted with the protein surface when using EAN as the precipitant [26]. Therefore, it is unclear whether ILs can generally act as precipitants for protein crystallization. Protein crystallization and phase behaviour with ILs present remains underexplored. In addition, although recent studies have investigated the interaction between common ions or small molecules with proteins or water molecules [34], there is little insight into how ILs interact with proteins at the atomic level.

To date, significant progress has been made in developing IL systems for modulating protein behaviour, usually focusing on model globular proteins such as lysozyme, ribonuclease A, cytochrome *c*, hemoglobin, and lipases [15,17,25,35–38]. In particular, hen egg white lysozyme is a frequently used model in studies of protein crystallization, protein binding, direct and reverse Hofmeister Series, and amyloid formation, since it is a well-folded and monomeric protein with distinct phase behaviour [12,39]. The protein phase separation and metal ion (e.g., Ca^{2+})-binding sites in eukaryotes have been extensively studied [40], however, with the simple lysozyme model, current understanding of specific ion effects on protein properties, interactions and ion binding is limited.

Here, we investigate lysozyme crystallization and phase behaviour, conformational changes, size and shape changes and aggregation in dilute to highly concentrated IL solutions as well as ion binding in crystallographic structures. To gain comprehensive insights, we have used a multi-technique biophysiochemical approach, combining spectroscopic methods, activity assays, X-ray crystallography and SAXS. Our focus centers on two ILs, namely EAN and ethanolammonium formate (EtAF), with other salts and ILs included for comparison. The crystallographic structures unveil the molecular mechanisms underlying the interaction and ion binding between the ILs and protein, providing unprecedented insights into the interfacial phenomena associated with protein ion binding. We emphasize the specific ion effects and the effect of ion binding on the protein biochemical properties.

2. Results and discussion

2.1. Phase diagram and crystallization of lysozyme in ILs

The four key IL-water states are highlighted in Fig. 1a, since water addition is important to hydrate proteins. We classify IL-water systems as dilute, intermediate, hydrated, and neat, based on IL concentrations. To consider the total ion numbers in the whole system, we present the unit of molar percent for all ILs, which can be converted to molarity and weight percent (Table S1). However, it should be noted that the concept of pH is only valid in dilute and intermediate IL concentrations (i.e., low concentrations) with up to ~ 17 mol% IL. The two main ILs, namely EAN and EtAF, were used in this work (Fig. 1b), since they have simple ion-combinations and can maintain lysozyme activity and structure [23,26,41]. The pH of low concentrations of EAN and EtAF was 5 and 8, respectively, and both were adjusted to 8. For the acid-base properties of hydrated or neat ILs (i.e. high concentrations), EAN is slightly acidic and EtAF is neutral [42,43].

The phase diagram and the solubility of lysozyme in the two IL-water mixtures was determined at various protein and IL concentrations (Fig. 1b and Table S2). The results show that the two ILs are effective crystallizing agents, in contrast to previous studies using ILs as co-precipitants [28,44]. Since the solubility line is commonly in the metastable zone [45], it divides the phase diagram into soluble, nucleation, metastable and precipitation zones.

Lysozyme had a consistent solubility of 220 ± 15 mg/mL in water and 258 ± 17 mg/mL in buffers at pH 4–8 (control samples, Table S2). In the low IL concentration range of 1–5 mol% EAN, the lysozyme solubility decreased significantly to 8–15 mg/mL (Fig. 1b). The solubility then increased until a maximum of ~ 300 mg/mL was reached in the highly hydrated IL state, i.e., ~33 mol% EAN, which corresponds to two water molecules for one ion pair. Remarkably, this molar ratio of 2:1 is the highest ionic strength for protein crystallization reported in the

literature, although we noted some lysozyme aggregates (Fig. S1). Further increasing the EAN concentration to 50–100 mol% IL caused a decrease in protein solubility to ~100 mg/mL, with only lysozyme precipitates observed. Note that lysozyme solubility was determined using the Protein A280 method only at low IL concentrations (*red points*, Fig. 1b) owing to IL-induced high 260/280 values at higher IL concentrations (Table S2).

In contrast, the EtAF solutions led to a relatively constant lysozyme solubility of ~ 10 mg/mL across all IL concentrations (Fig. 1b). The EtAF concentration limit for lysozyme crystallization was 33 mol%, similar to EAN. We also found that the solubility of lysozyme in 5 other ILs at 17 mol% was between 50 and 164.4 mg/mL (Table S2), which was lower than EAN, and no lysozyme crystals were observed. Owing to the remarkable changes in lysozyme solubility, the two ILs acted as strong precipitants. In both low and high protein concentrations, the two ILs affected the protein aggregation kinetics and crystal morphology (Fig. 1c). At 17 mol% and over, the crystal packing became inhomogeneous, and aggregates were present (Fig. S1). This possibly led to the aggregation and nucleation in a protein-rich dense droplet. We also found that pH was not critical for lysozyme crystallization, with crystals still forming in EAN solutions of pH 2 (Fig. S1), suggesting that high IL/salt concentrations are critical.

Overall, the crystallization and nucleation process in ILs at low lysozyme concentrations is consistent with classical nucleation theory, including the IL-dependent saturation, formation of unstable and ordered clusters, nucleation, and crystallization [46]. However, at high protein concentrations, the process is related to two-step nucleation theory, comprised of formation of an aggregated protein-rich dense droplet, followed by nucleation inside the droplet and crystallization [46]. Note that this protein-rich dense droplet is unstable, and under a higher free energy than a dilute droplet. We observed that both ILs at dilute, intermediate and hydrated concentrations promoted the aggregation during the nucleation, when the protein concentration was above the solubility limit.

2.2. Lysozyme activity, size and structure changes at low and high IL concentrations

Next, we evaluated lysozyme activity in different solvents. To compare the anion and cations, we introduced two other cations of butylammonium (BA) and hexylammonium (HA) coupled with the nitrate anion (Fig. 2a), along with sodium salts ($NaNO_3$, NaCOOH and NaCl), for comparing a metal cation with protic ammonium cations. The six PILs include EAN, BAN, ethanolammonium nitrate (EtAN), HAN, EtAF and ethylammonium formate (EAF). The relative lysozyme activity was mostly maintained in 0.25 mol% IL or salt solutions, within the first 10 min (i.e., initial rate) compared to buffer, except for EAF with only ~ 10% activity (*top panel*, Fig. 2b). However, no activity was detected within 10 min in 1 mol% solutions and higher, indicating even dilute IL concentrations inhibit the enzyme activity. We then monitored the activity assay for 10 h for both 0.25 and 1 mol% solutions (Fig. S2). The assay was completed within 2 h for lysozyme in 0.25 mol% ILs. In the 1 mol% IL solutions, it was significantly longer, with the relative activity of the four nitrate-based ILs close to 50 %, and the activity in $NaNO_3$ comparable to the buffer (*bottom panel*, Fig. 2b). This suggests that the cation has a significant effect, especially when comparing the ammonium cation with a metal cation, as discussed in previous work [6]. Conversely, there was little difference in lysozyme activity when comparing ILs with different alkyl chain lengths on the ammonium cation, namely EAN, BAN and HAN, consistent with the maintained lysozyme structure at dilute IL concentrations [47]. Again, a remarkable difference in lysozyme activity in EtAF (~75%) and EAF (~20%) highlights the cation effect. The hydroxyl group present on EtAF may aid in maintaining the activity of lysozyme, while EAF tends to denature the lysozyme [24,41]. Interestingly, the activities in EtAN with EAN were comparable, suggesting that the nitrate ion has a dominant effect. The enzyme showed the highest activity in 1 mol% solutions of EtAF and the three sodium salts.

To verify the different effects of EAN, EtAN, EtAF, EAF and three common salts, we studied the size and structural change of lysozyme using SAXS. The radius of gyration (R_g) of lysozyme in the seven solutions at 0.25 and 1 mol% were compared with buffer (Fig. 2c and S3).

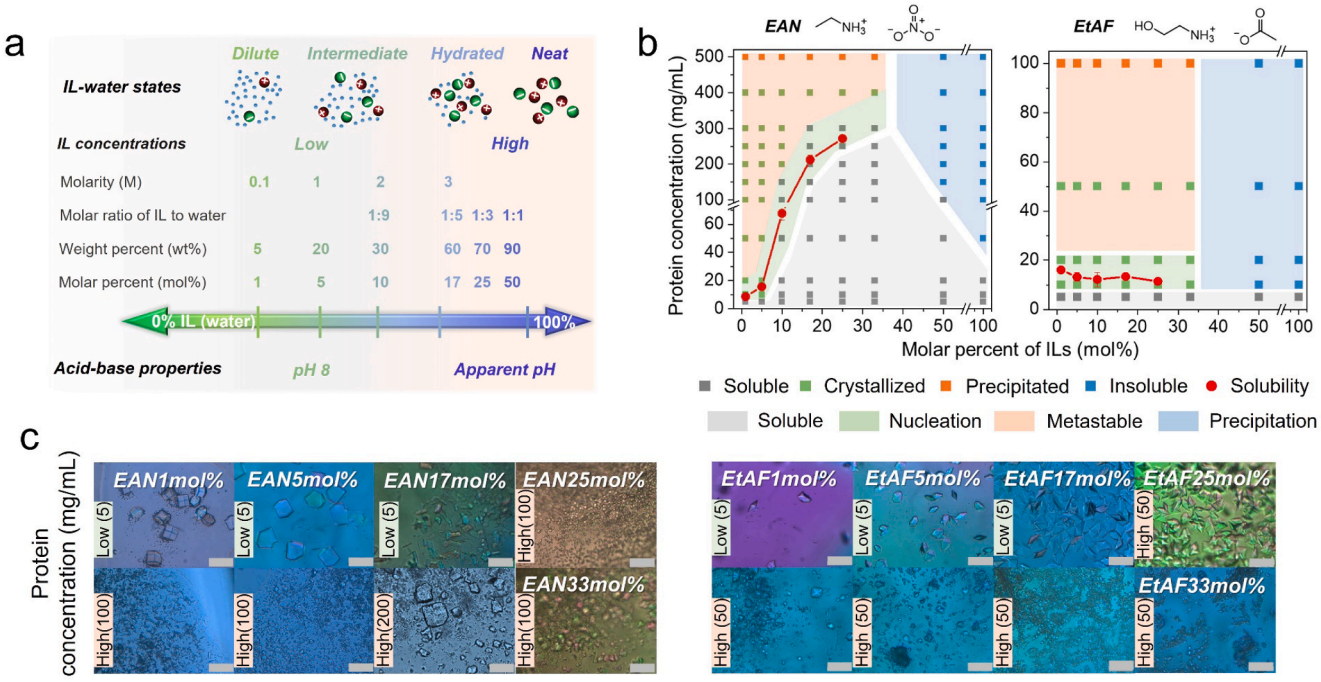

Fig. 1. (a) Four key IL-water states, different units correlated with IL concentrations, and their acid-base properties. (b) Lysozyme phase diagram in EAN and EtAF as a function of IL concentration. (c) Microscopy images of lysozyme crystals in IL-water mixtures with low and high protein concentrations. Scale bar, 1 μm.

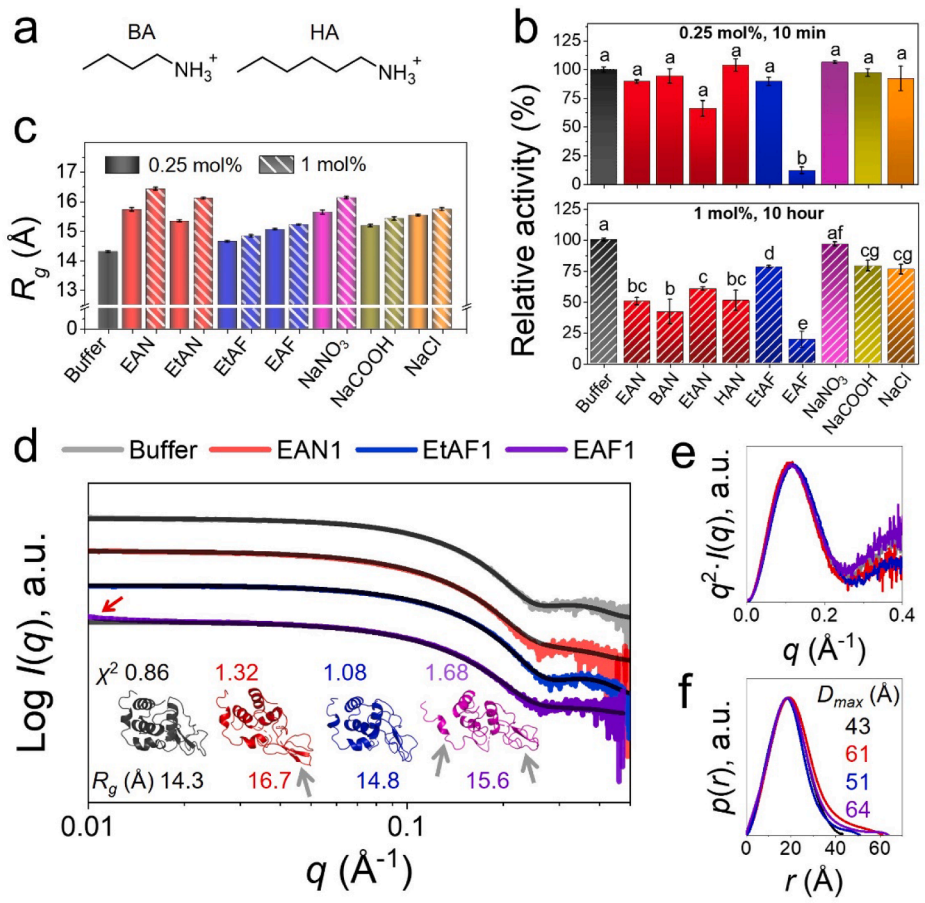

Fig. 2. (a) Cations of butylammonium (BA) and hexylammonium (HA) to form BAN and HAN. (b) Relative activity of lysozyme in PILs and salts compared to buffer (100%). Different letters on bars indicates significant difference ($p < 0.05$). (c) The R_g values (Å) of lysozyme in buffer, PILs and salts. (d) SAXS patterns of lysozyme in buffer, ILs at 1 mol% overlaid with SREFLEX fitting curves using PDB 7JMU. The insert shows the SREFLEX models and their χ^2 and R_g values. The red arrow shows a small upturn in low q region of EAF pattern, while grey arrows indicate the significant conformational changes in loop regions. (e) The Kratky plots and (f) $p(r)$ plots and D_{max} values of lysozyme in the solutions.

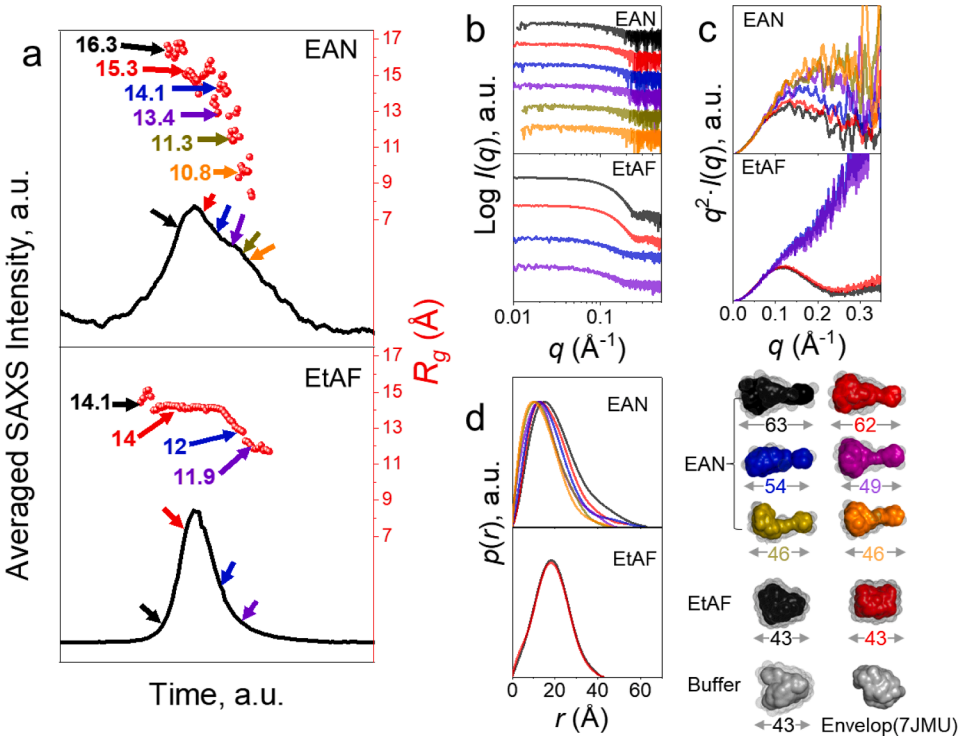

Fig. 3. (a) SEC-SAXS profiles with the average SAXS intensity and the R_g corresponding to each pattern as a function of time. The colored arrows show the lysozyme species with their R_g values for further analysis. (b) SAXS patterns and (c) Kratky plots of EAN or EtAF-treated lysozyme species collected from SEC. (d) The $p(r)$ plots of lysozyme species and GASBOR models (solvents shown in grey mesh) with their D_{max} values provided. The two EtAF-treated species in blue and purple color cannot generate meaningful $p(r)$ and D_{max} data.

The R_g values in EAN, EtAN and $NaNO_3$ were around 15.5 at 0.25 mol% and over 16 Å at 1 mol%. The values in EtAF (14.6 and 14.8 Å at 0.25 and 1 mol% EtAF, respectively) were similar to that in buffer (14.3 Å), while in EAF, NaCOOH and NaCl it increased by approximately 1.5 Å. The amount that R_g changed follows the order of EtAF, NaCOOH, NaCl, EtAN, $NaNO_3$ and EAN, which is likely to correlate to lysozyme size and structural changes. The R_g changes in EAN and EtAN may also be due to the nitrate binding in the hydration layer of the protein [26]. As reported, SAXS measures the hydrated protein molecules (generating an ~ 3 Å layer of water with higher density) as a complete object[48].

The SAXS patterns of lysozyme in EAN, EtAF and EAF were further fitted and refined based on lysozyme structure (PDB 7JMU) using SREFLEX [49], revealing that the lysozyme structures were generally maintained in the three ILs (*inset*, Fig. 2d). EAF resulted in more conformational rearrangement in the loop regions and a small degree of aggregation (a small upturn in low q region of EAF SAXS pattern). The bell-shaped distribution of the Kratky plots show that lysozyme has similar flexibility and globular structure in the buffer and three IL solutions (Fig. 2d), while the extended tail of the distance distribution functions ($p(r)$) plot in all three IL samples demonstrates that lysozyme was more elongated with ILs present (Fig. 2e). Lysozyme in EAN and EAF both have the longest tails in the high r region in $p(r)$ plot (Fig. 2f), consistent with their extended structure in the SREFLEX models. However, the lysozyme activity loss in EAF can be related to the changes in loop regions and a small degree of aggregation rather than the small R_g change, since R_g changes in EAF were smaller than that in EtAF and EAN.

To explore the effect of highly concentrated ILs, a further SAXS study was conducted by incubating lysozyme in neat ILs (EAN or EtAF-treated), and then subsequently running them through size-exclusion chromatography (SEC)-SAXS with buffer. Species were present with different R_g values, varying from ~ 10 to 17 Å for EAN-treated lysozyme, and 12 to 14 Å in EtAF-treated lysozyme (*arrows*, Fig. 3a). This indicates that some of the protein aggregation and structural changes are irreversible, and lysozyme can be more aggregated and unfolded in neat EAN than EtAF. FTIR and circular dichroism spectra further showed that neat EtAF had less effect than EAN on the secondary structure of lysozyme with 1 and 7-days incubation (Fig. S4). Additionally, neat EAN with two apparent pH values showed a similar effect on lysozyme structural changes, confirming the EAN effect was primarily due to the IL nature rather than the apparent pH, and that the structural changes induced by EAN were irreversible (Fig. S4). The different lysozyme species were then analyzed based on their SAXS patterns (Fig. 3b). The Kratky plots of lysozyme species with R_g 14–16 Å showed standard bell-shapes in both EAN and EtAF (*black and red curves*, Fig. 3c). However, species with lower R_g values (<14 Å) had increased intensity in the high q region in both ILs, indicating the species were unfolded, and was much more remarkable in EtAF. Note that the R_g values calculated by Guinier method is restricted to the data in the low q region, leading to the smaller R_g for some lysozyme species. However, the maximum dimension D_{max} obtained from a $p(r)$ plot utilizes the entire dataset to consider the real space electron density, and hence gives more insight into shape changes. The $p(r)$ data was employed for *ab initio* reconstruction of the protein structure by a chain-like ensemble of dummy residues using GASBOR [50] (Fig. 3d and Fig. S5). The protein species in EAN were all elongated with D_{max} between 46 and 63 Å (*top panel*, Fig. 3d), while the two lysozyme species in EtAF maintained a globular shape (D_{max} ~43 Å) (*bottom panel*, Fig. 3d). A small portion of species with significant structural changes are noted, suggesting EtAF still induced irreversible aggregation and structural loss (Fig. S5).

Table 1
Details of crystallography parameters of lysozyme crystallized in the presence of ILs.

ILs	EAN 1 mol% (*ca.* 6 wt%)	EAN 5 mol% (*ca.* 24 wt%)	BAN 1 mol% (*ca.* 7 wt%)	EtAN 1 mol% (*ca.* 7 wt%)	EtAF 5 mol% (*ca.* 20 wt%)	EtAF 7 mol% (*ca.* 30 wt%)	EtAF 17 mol% (*ca.* 50 wt%)
PDB ID	7JMU	7RXY	7RYD	7RYK	7RZ2	7RZ0	7RZ1
Resolution range (Å) [a]	43.23–1.20 (1.22–1.20)	29.84–1.60 (1.64–1.60)	17.09–1.18 (1.20–1.18)	29.75–1.76 (1.80–1.76)	24.29–1.07 (1.10–1.07)	38.40–1.38 (1.42–1.38)	54.20–2.05 (2.10–2.05)
Space group	$P12_11$	$P12_11$	$P12_11$	$P12_11$	$P41\ 21\ 2$	$P41\ 21\ 2$	$P41\ 21\ 2$
Cell dimensions a, b, c (Å)	27.58, 62.64, 59.65	27.53, 62.48, 59.64	27.64, 62.45, 59.78	27.46, 62.35, 59.47	76.76, 76.76, 38.57	76.79, 76.79, 38.31	76.65, 76.65, 38.29
Unit cell angles α, β, γ(°)	90.00, 90.54, 90.00	90.00, 90.26, 90.00	90.00, 90.21, 90.00	90.00, 90.57, 90.00	90.00, 90.00, 90.00	90.00, 90.00, 90.00	90.00, 90.00, 90.00
Number of unique reflections [a]	60,485 (2781)	26,661 (179)	67,030 (415)	19,931 (158)	50,880 (371)	23,925 (199)	7645 (127)
R_{sym} or R_{merge} [a]	0.043 (0.313)	0.509 (0.060)	0.090 (0.029)	0.053 (0.017)	0.096 (0.066)	0.113 (0.070)	0.270 (0.050)
Multiplicity or redundancy[a]	6.9 (6.0)	6.3 (5.1)	2.0 (1.7)	1.9 (1.8)	13.4 (10.2)	13.9 (10.0)	19.2 (14.1)
Completeness (%) [a]	95.5 (85.2)	99.9 (97.9)	99.8 (97.6)	99.9 (99.0)	99.4 (98.3)	100.0 (99.7)	100.0 (99.8)
Mean I/σ [a]	19.5 (3.9)	10.1 (16.7)	5.4 (13.7)	8.5 (18.5)	14.3 (28.9)	16.2 (26.8)	11.3 (24.4)
Mean CC (1/2) [a]	0.999 (0.938)	0.999 (0.999)	0.992 (0.995)	0.996 (0.998)	0.999 (0.993)	0.998 (0.998)	0.981 (0.999)
Refinement statistics							
R_{work}	0.145	0.140	0.203	0.137	0.150	0.144	0.160
R_{free}	0.179	0.207	0.233	0.226	0.172	0.176	0.243
Number ofnon-hydrogen atoms	2781	2245	4332	4286	2509	2209	2240
protein	4060	2049	4145	4075	2366	2075	2111
water	254	144	139	163	123	114	106
nitrate ion	60	52	48	48	19	19	23
Protein residues	254	254	254	254	127	127	127
RMS (bonds)	0.0196	0.0136	0.0151	0.0111	0.0195	0.0163	0.013
RMS (angles)	2.19	1.85	2.02	1.64	2.38	1.98	1.75
Ramachandran favored	98.08%	97.24%	96.06%	97.24%	98.43%	98.43%	95.28%
Ramachandran allowed	1.57%	2.76%	3.94%	2.76%	1.57%	1.57%	4.72%
Ramachandran outliers	0.39%	0%	0%	0%	0%	0%	0%
Rotamer outliers (%)	0.46	1.39	0.9	2.28	1.55%	1.79	5.31
Clashscore	0.97	2.94	3.09	2.43	4.54	3.31	6.48
Average B-factor	15.71	21.59	14.02	19.94	8.02	8.4	15.76
macromolecules	16.03	24.24	15.74	22.21	10.1	11.13	18
nitrate ion	28.56	42.67	28.19	38.24	14.99	17.77	30.61
water	24.61	35.46	25.44	30.94	22.22	23.64	32.67

[a] Highest resolution shell shown in parentheses.

2.3. Ion binding of ILs

Given that EAN and EtAF showed contrasting effects, we employed crystallography to understand the structural changes and IL-protein interactions in detail. We determined the lysozyme structure in 5 mol % EAN, 1 mol% EtAN and BAN, and 5, 7 and 17 mol% EtAF at resolutions between 1 and 2 Å (Table 1 and Fig. 4). Our recent lysozyme structure in 1 mol% EAN was included for comparison [26]. Firstly, we note that only EAN induced a precipitation-dissolution-crystallization process (Fig. S6a, b). In the four lysozyme structures with nitrate-based ILs present, more than 10 nitrate ions were identified in molecules A and B of the asymmetric unit. Interestingly, no cations were found (Fig. 4a), indicating nitrate binding is dominant. Ten binding sites were identified as occurring 3 or 4 times across all four structures, i.e., 3/4 or 4/4, indicating a high degree of conservation. These sites were defined as specific nitrate binding sites (*red labels*, Fig. 4a, b). Most of the nitrate ions preferred the positively charged side chains (R114, K33, R14, H15) and aromatic side chains, (F34, Y23, F38, F3, Y53, W62, W63, W111, W123). These interactions with aromatic side chains explain the quenched fluorescence of lysozyme and green fluorescence protein [26,27], and possibly led to Trp degradation [51] as a yellow colored solution was noted in EAN (Fig. S6c). It is intriguing that three specific binding sites including **A2/B2**, **A5/B6**, and **A6/B7** were also conserved when compared the two molecules (A and B) in the unit cell, for the four structures (Fig. 4a). Importantly, the first two selectively bound to all four structures with the same side chains, i.e., Q121, I124 and S24 for **A2/B2** and F3, R14, H15 and D87 for **A5/B6** (Fig. 4b). On the other hand, we identified five formate anions in three lysozyme structures crystallized with EtAF (Fig. 4c). In contrast to EAN, we identified at least one ethanolammonium cation in the structure (**4** and **5**). Interestingly, the cations all presented as an ion pair with the formate anion interacting with negatively charged side chains, E7, E35 and D52 (Fig. 4d). Moreover, the EtAF ion pair was in the cleft of the active site, namely, E35, D52, R63 and A107, though this binding did not affect its enzyme activity. Regarding the formate anion, most formate anions generally interacted with positively charged arginine groups in lysozyme, i.e., R5, R14, R114, R128. Two specific formate bindings, namely **1** and **4**, are identical to the nitrate bindings of **A2/B2** and **A5/B6**, respectively (*blue* and *orange frames*, Fig. 4b and d). When superimposing all the 11 protein molecules from the 7 PDB structures, three conserved specific binding sites for nitrate and formate is noted (**A2/B2/1**, **A5/B6/7** and **A9/B8/6**, Fig. 4e).

Further, the electrostatic surface graphs show that the binding generally favors the concavities, especially positively charged areas (Fig. 4f and S7). Specifically, polar residues of Ser (S), Tyr (Y) and Asn (N) and positively charged residues, particularly Arg (R), are preferred for interactions. The hydrophobic or basic residues also participated in the interactions, including Ile (I), Ala (A), Phe (F), Trp (W), Gly (G) and Pro (P) with nitrate ions, and I, Val (V), A and W with formate ions. Notably, both nitrate and formate anions perturb a universally conserved salt bridge in close proximity to R14, H15, and D87, consistent with phosphate binding, which is known to be kosmotropic [52]. Overall, over 50% of the anion-lysozyme contacts comprise hydrogen bonds or electrostatic interactions involving the basic R, polar N, and aromatic W residues (specifically for nitrate), indicating that these residues provide favorable environments for these anions.

Additionally, a comparison of interactions between the water molecules and ILs, that are tightly bound on the protein surface (in the first hydration layer), shows that not all ions were participating in hydrogen bonding with water molecules, but that all ions interacted with the

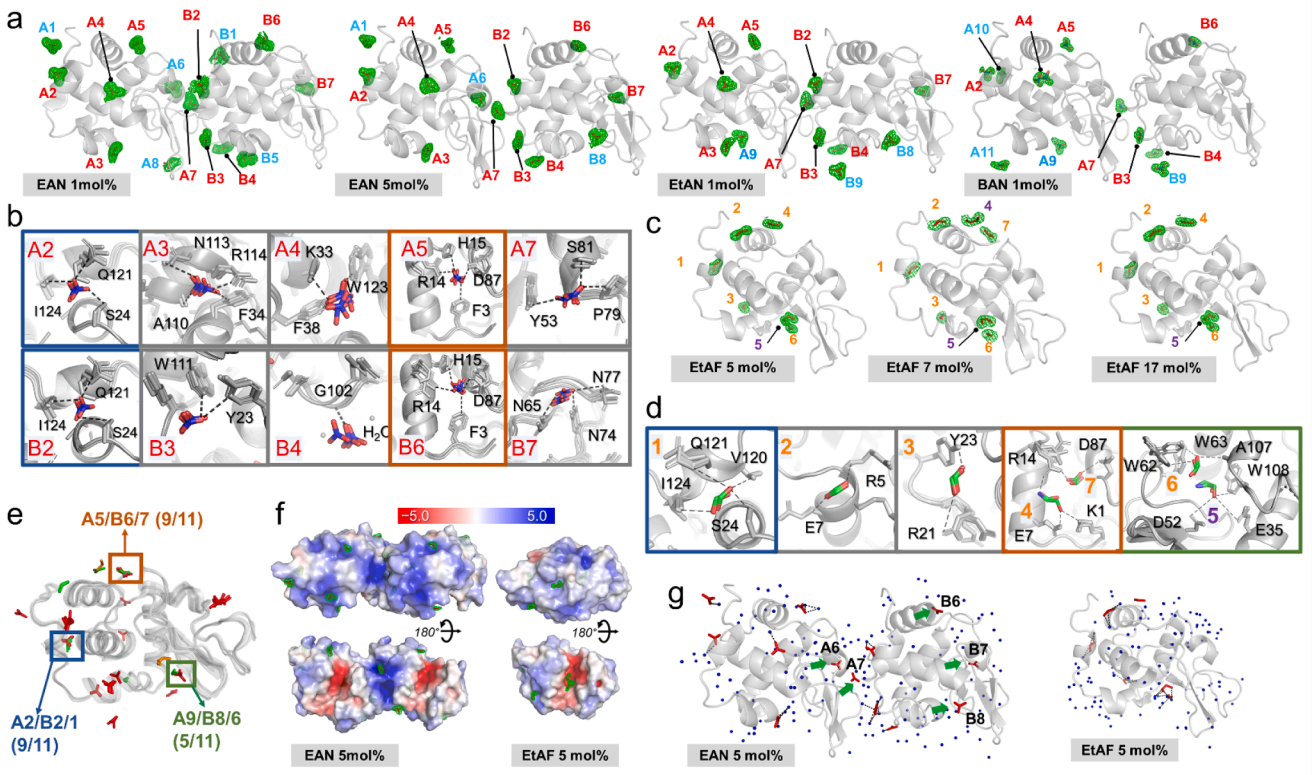

Fig. 4. (a) Lysozyme structures in nitrate-based ILs with omit maps (green) of the nitrate ions. Specific binding occured 3 or 4 times in the four structures (3/4 or 4/4) = red, binding of 2/4 or 1/4 = blue. (b) The specific nitrate binding (3/4 or 4/4) interactions with lysozyme side chains. (c) Lysozyme structures in EtAF with omit maps (green) of the ions. (d) Specific interactions between formate (3/3, orange) and ethanolammonium (3/3, purple) with lysozyme side chains. (e) Superimposion of all 11 lysozyme molecules and the specific anion binding sites (blue, orange and green frames and labels in b and d). (f) Electrostatic lysozyme surface potential with the omit maps of ions in EAN and EtAF at 5 mol%. Red = negative potentials, blue = positive potentials. (g). Hydrogen bonding of ILs with water molecules (blue dots). Green arrows = ions without interaction with water molecules.

protein backbone or side chains mainly by hydrogen bonds (Fig. 4g and S8). This suggests a preferential binding of ions to the protein surface rather than the hydration layer, similar to the behaviour of GuaCl, which minimally disrupts the water structure [53]. The observed number of water molecules in lysozyme-EAN structures was ~ 150, and lysozyme-EtAF structures had ~ 120 (Table 1). This difference may be because of a moderate favoring of water by the nitrate anions and the effect of crystal packing forces. An evident decrease of water molecules from 123 to 106 was observed with increasing the EtAF concentration from 5 to 17 mol %, indicating a slight disturbance from IL ions on the first hydration layer as a function of ion concentration. This is consistent with previous literature showing mobile ions compete with lysozyme for water, thus altering the availability of water in the first hydration layer at high ionic strength [54]. However, crystallographic water molecules may not be an accurate representation of the dynamic hydration layers that exist in solution. It is important to note that increasing IL concentration can dramatically increase protein solubility and even promote crystallization, which was unattainable with common or buffer salts. Thus, it is highlighted that ILs can be used in protein crystallization, not only as additives, but also as a co-solvent with water, and are able to drive, favor, and sustain protein crystallization.

We then superimposed all 11 protein molecules and observed that the specific ion binding of ILs had minimal effect on protein structural changes (Fig. 5a). The helical and beta regions were well-preserved, consistent with the SREFLEX models (Fig. 2d). However, slight conformational changes in loops I near R128 and loops II (residues 41–79, particularlly N65, N74 and S81) were observed in the presence of nitrate-based ILs, which possibly resulted from ion binding of nitrate **A1** and **A7** and **B7**. Further, we compared 9 additional PDB structures and the ion binding patterns on 23 lysozyme molecules (Fig. 5b and c), in the presence of chloride [55–57], nitrate [58,59], sulfate [60], phosphate [52], along with cations such as sodium and guanidium [61]. Notably, these studies employed dilute salt solutions along with complex crystallization agents, which differ from our study that solely utilized ILs. Despite these variations, the overall structure of lysozyme remained largely conserved across all 23 structures (Fig. 5b). Intriguingly, only nitrate induced the changes in loops I and II when using $NaNO_3$, EAN, EtAN, or BAN, owing to the interactions with the charged and polar side chains in those regions. By examining the occurrence of ions in the respective structures, we identified eight specific anion binding sites and one cation binding site (**1**–**9**, Fig. 5b-d and S9). These anion binding sites consisted of three sites for NO_3^- (coresponding to **A3**, **A7** and **B7** sites in Fig. 4b), four for other anions (primarily NO_3^-, $HCOO^-$ and Cl^-, corresponding to binding sites of **A2**, **A5**, **A4**, **A9** and **4** (Fig. 4b and d). A summary of ion binding on the side chains is presented in Fig. 5d. Notably, except for site 4, all anion binding sites included nitrate ions, and hence nitrate had more binding sites than other ions, with its preferential interactions involving charged and polar residues of W, R, S, Q and N.

Furthermore, we observed that the salts and ILs affected the crystal packing in a similar way, regardless of ion concentration. Specifically, NaCl and EtAF generally led to tetragonal lattices ($P4_32_12$), whereas

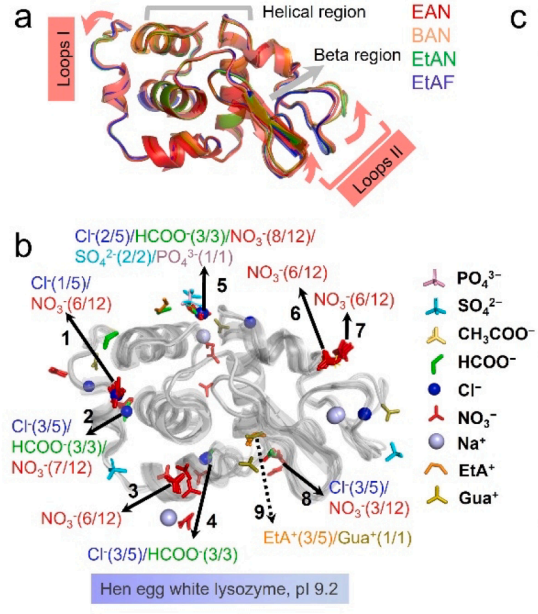

c

PDB	Resolution (Å)	Crystallization method and agents[a]	Space Group	Ion binding (amount)[b]	Ref
1DPX	1.65	VD: 5wt% NaCl	$P4_32_12$	Cl^-(2)	[55]
1IEE	0.94	CD: 20wt% NaCl	$P4_32_12$	Cl^-(5), Na^+(1)	[56]
1LKS	1.10	BC: 5wt% $NaNO_3$	$P1$	NO_3^-(6)	[58]
2VB1	0.65	VD: 8.5wt% $NaNO_3$, 20% EG	$P1$	EG(3), NO_3^-(9)	[59]
3WL2	0.96	VD: 3.4wt% $NaNO_3$, 20% EG	$P12_11$	A-NO_3^-(2), Na^+(1); B-NO_3^-(8), Na^+(1)	N.A.
5WRA	1.45	SC: 28wt% NaCl, 8wt% PEG6000	$P4_32_12$	Cl^-(1), Na^+(1)	[57]
6A10	1.13	VD: 16wt% $(NH_4)_2SO_4$	$P1$	A-SO_4^-(3); B-SO_4^-(3); C-SO_4^-(4)	[60]
6A4N	1.75	VD: 8.2wt% NaCl, 24wt% GuaCl	$P4_32_12$	Cl^-(6), Na^+(1), GUA^+(5)	[61]
6F1L	1.30	VD: 2.9wt% NaCl, 2wt% Na_2HPO_4/NaH_2PO_4	$P2_12_12$	PO_3^{2-}(1), Cl^-(1)	[52]
7JMU	1.20	BC: EAN 1mol% (7%)	$P12_11$	A-NO_3^-(7); B-NO_3^-(8)	[26]
7RXY	1.60	BC: EAN 5mol% (24%)	$P12_11$	A-NO_3^-(7); B-NO_3^-(6)	This work
7RYD	1.18	BC: BAN 1mol% (7%)	$P12_11$	A-NO_3^-(8); B-NO_3^-(3)	This work
7RYK	1.76	BC: EtAN 1mol% (7%)	$P12_11$	A-NO_3^-(6); B-NO_3^-(6)	This work
7RZ2	1.07	VD: EtAF 5mol% (20%)	$P4_32_12$	$HCOO^-$(5), EtA^+(1)	This work
7RZ0	1.38	VD: EtAF 7mol% (30%)	$P4_32_12$	$HCOO^-$(5), EtA^+(2)	This work
7RZ1	2.05	VD: EtAF 17mol% (50%)	$P4_32_12$	$HCOO^-$(5), EtA^+(1)	This work

[a] EG = ethylene glycol, VD = vapor diffusion, CD = counter diffusion, BC = batch crystallization, SC = serial crystallography. The buffer salts (<1wt%) and pH was not provided.
[b] The ion binding per protein molecule in a unit cell (A, B or C) are listed.

d

Ion binding sites	Side chains
1 (anions)	K33, W123
2 (anions)	S24, Q121
3 (NO_3^-)	N113, R114
4(anions)	R21, Y23
5 (anions)	R14, H15, D87
6 (NO_3^-)	S81, N65
7 (NO_3^-)	N65, N74
8 (anions)	W62, W63
9 (EtA^+, Gua^+)	Q57, A107, W108

e

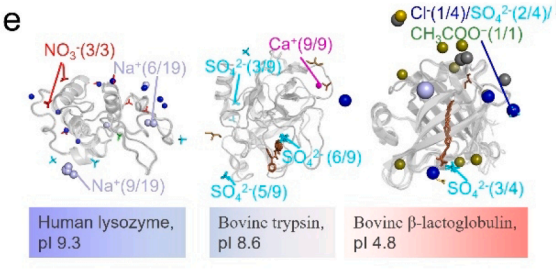

Ion binding sites	Side chains
Human lysozyme (NO_3^-)	R5
Human lysozyme (NO_3^-))	S24, N27, R122
Human lysozyme (Na^+)	S61
Trypsin (SO_4^{2-})	K174, G174
Trypsin (SO_4^{2-})	T125, S127
Trypsin (SO_4^{2-})	Q192, S195
Trypsin (Na^+)	E70, N72, V76, E80
β-Lactoglobulin (SO_4^{2-})	K69, L87
β-Lactoglobulin (Cl^-/SO_4^{2-})	T76, K77, K83

Fig. 5. (a) Superimposed 11 lysozyme molecules reported in tihs work. (b) Superimposed 23 lysozyme molecules from 16 PDB structures showing 9 specific ion binding sites labelled by colors. The dashed line indicates cation binding, and the solid lines refer to anions. (c) Lysozyme PDB structures and their statistics, including space group and amount of ion binding. (d) Summury of primary ion binding in the nine binding sites. (e) Ion binding analysis for 19 human lysozyme, 9 bovine trypsin and 6 bovine β-lactoglobulin molecules, and the summary of primary ion binding sites. The numbers in the bracket refer to the times ions appeared among the number of PDB structures with corresponding ILs/salts.

nitrate and sulfate led to monoclinic ($P12_11$) or triclinic ($P1$) lattices (Fig. 5c). However, most previous studies utilized complex additive formulations, leading to the variations of space groups. In contrast, when only using ILs, lysozyme had a monoclinic lattice ($P12_11$) in nitrate-based ILs, consistent with a previous study showing monoclinic packings were favored with large monovalent ions of low charge density such as I^-, NO_3^- and SCN^- [62]. This indicates that anions generally modify intermolecular contacts and crystal packing in liquid/solid forms of the protein.

Since the specific ion binding of lysozyme is dominated by the anions, we further investigated this phenomenon in other proteins by analyzing reported PDB structures of human lysozyme, bovine trypsin and bovine β-lactoglobulin, which have different isoelectric point (pI) and thereby different surface charges (Fig. 5e, S10 and Table S3). Two binding sites of NO_3^- and Na^+ are both noted in human lysozyme. Three SO_4^- and one Ca^{2+} binding sites are found in trypsin, while one SO_4^- and one anion binding in β-lactoglobulin. Although human lysozyme has a similar surface charge as hen egg white lysozyme, it displayed less specific binding for nitrate. However, similar binding sites for anions and Na^+ were identified, indicating the binding pattern may be protein-independent. When comparing the two types of lysozyme (~60% sequence similarity), the interactions between nitrate and side chains of R (positively charged), S and N (polar) are generally preferred. For example, nitrate binding on S24 is conserved. Trypsin can be slightly alkaline, and three SO_4^- and one Ca^{2+} binding on polar residues (e.g, K and S) were observed. Although β-lactoglobulin can be mostly negatively charged, the electrostatic interactions of SO_4^- and anions Cl^-/SO_4^{2-}/CH_3COO^- with positively charge residue K were noted, along with a few cation interactions. Overall, anion binding appeared to be dominated by polar contacts and favored electrostatic interactions, irrespective of pH and pI. it is important to note that the existing literature on ion binding is limited, and nitrate binding was not found in trypsin and β-lactoglobulin. Further studies investigating ion binding modulation with a wider range of ion combinations and concentrations, particularly for ILs, are warranted to expand our understanding in this area.

2.4. Specific ion effects, hydration and interactions

Based on the anions evaluated in Fig. 5 and the previously established specific ion effects, the order of anions is $\boldsymbol{SO_4^{2-} > CH_3COO^-, HCOO^- > Cl^- > NO_3^-}$ (Fig. 6a). However, there is no obvious trend for

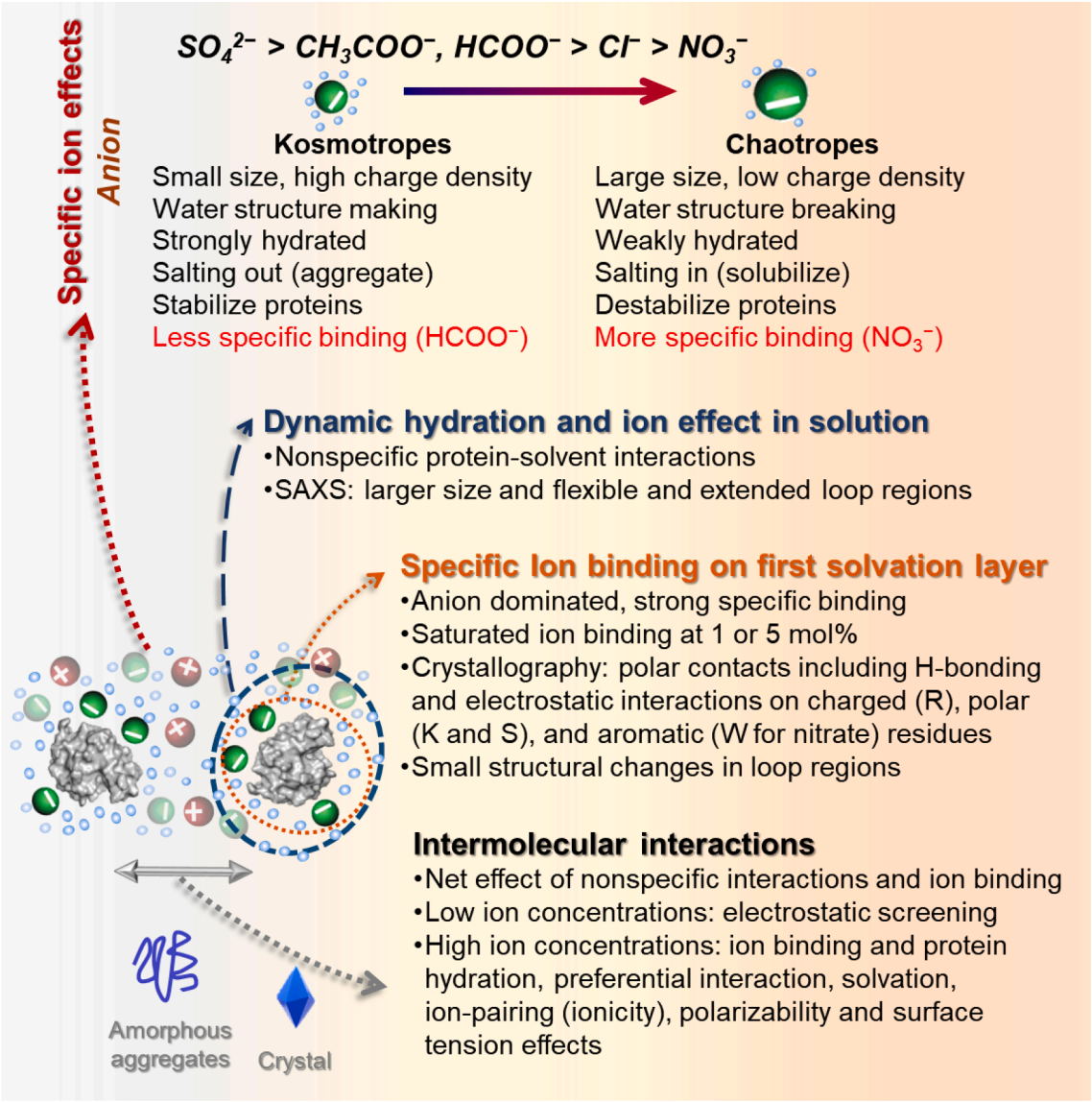

Fig. 6. Scheme of the correlation of specific ion binding of proteins with specific ion effects, hydration and inter-species interactions.

cations, since there was less binding observed for common metal cations like Na^+ and Ca^{2+} with the proteins. We highlight that the anion-binding is critical to the series where Kosmotropes induced less specific binding and Chaotropes had more binding. It is worth noting that lysozyme, being a well-studied model protein, exhibits an inverse anionic Hofmeister series at very low ion concentrations (typically < 0.1 or 0.2 M, *ca.* 0.25 mol%). This is attributed to dominant nonspecific electrostatic interactions with the protein/water interface [39,63]. Such interactions can be relatively strong and saturated after the addition of ~ 0.5 M salts (*ca.* ≥ 1 mol%) [39]. This attribution can also be applied to ILs, since they can exhibit high dissociation similar to conventional salts at low concentrations [64]. Considering we used relatively high salt/IL concentrations, we focus discussion on the direct Hofmeister series herein. It is generally accepted that small ions with high charge density (e.g., SO_4^{2-}, carboxylate) are strongly hydrated (kosmotropes) and result in the salting out of proteins [65]. Direct interaction of these small ions with charged groups requires desolvation which is enthalpically unfavorable, although these ions may have an indirect effect mediated by intervening water molecules[53]. Consequently, small ions with high charge density interact minimally with proteins and encourage the protein to minimize its solvent accessible surface area. Previous studies have shown that strongly hydrated SO_4^{2-} and PO_4^{3-} are preferentially excluded from the surface of proteins, with only one phosphate ion binding site reported on lysozyme [52,66]. However, monovalent ions of low charge density (e.g., Cl^-, NO_3^-) are weakly hydrated (chaotropes) and are likely to directly bind to proteins thereby decreasing the net charge of the positively charged lysozyme. This results in salting in behaviour, with direct interactions occurring primarily with charged groups of amino acids and influencing the intermolecular forces among protein molecules. However, when correlating the effect of specific ion binding of ILs with the specific ion effects, hydration and interactions in this study, several points should be considered, as illustrated in Fig. 6. Note that we use specific ion effects instead of Hofmeister series in the following context, due to the controversy associated with the Hofmeister series origin and applicability for ILs [15].

For the ion binding in the hydration layers of the protein, the interfacial water surrounding a protein can be divided into three layers: the solvation layer, the transition layer, and the bulk layer [65]. The solvation layer and bulk layer are determined by protein nature and specific ion effects, respectively. However, ions and solvent molecules interact more strongly with the protein in the solvation layer. The specific ion binding we observed in crystallographic structures is in the solvation layer, and the ion molecules may not be an accurate representation of the dynamic hydration layers in solution, and can be affected by crystal packing forces. Nonetheless, the ion binding in protein hydration layers can be critical, as evidenced by the high number of specific ion-protein binding of nitrate, which likely contributes to the enhanced solubility, crystallization behaviour and destabilizing effect in EAN compared to EtAF (Fig. 2). In solutions, measurements of R_g and D_{max} by SAXS consider protein hydration layers, and we observed higher R_g values and flexible loop regions in SREFLEX models in the presence of EAN and $NaNO_3$ (Fig. 2), as well as larger D_{max} values with extended shape (GASBOR model) of lysozyme treated by neat EAN (Fig. 3). As discussed above, the flexible and elongated loop regions observed in solution can be largely attributed to the specific ion binding in loop I and II within the solvation layer. Conversely, EtAF exhibited less ion binding, although its ion pair was identified for the first time in the protein, interfering with a salt bridge in lysozyme and potentially playing a role in antigen–antibody interactions [67]. Furthermore, we observed that lysozyme in 5 mol% EtAF had similar ion binding as it had in 17 mol% EtAF, with increasing ion concentration slightly reducing the number of water molecules in the hydration layer observed in the crystal structures. This suggests that the ion binding in the solvation layer can be saturated at around 1 and 5 mol% with a slight disturbance in protein hydration with 17 mol% EtAF present. Further increasing the ion concentration can cause ions to compete with protein for water in the bulk phase, thus leading to a new effect (e.g., decrease in the interfacial tension) [39,54,68] and irreversible aggregation was observed in over 30 mol% ILs and neat ILs (Fig. 2 and 3).

Regarding interactions of ion binding, we highlight that the ion binding, especially for anions, on the protein surface are primarily driven by polar contacts including hydrogen bonding and electrostatic interactions. Nitrate ions exhibit more binding sites than formate and other ions in lysozyme, with important residues possessing charged, polar, and aromatic side chains. Similar specific ion binding is observed in other proteins with different isoelectric points (pI). However, the specific ion effects do not directly correlate with the amount of ion binding in different proteins, likely due to the limited availability of PDB structures with ions and the non-specific and unobserved nature of most ion binding in crystallographic structures, which mainly capture strong ion-protein interactions. In solution, especially at low and medium ion concentrations, the nonspecific interactions (mostly electrostatic) can be important [39]. Thus, the IL effect on lysozyme is attributed to the net effect of nonspecific protein-solvent interactions and the strong ion binding observed in crystal structures. Furthermore, as the lysozyme surface is overall positively charged and anions tend to interact more with the positively charged residues, the surface potential (i.e., effective surface charge density) of the protein/water interface can be reduced, known as the electrostatic screening effect of anions on the protein. In contrast, cations exhibit weaker binding, even for Ca^{2+} which gave the highest binding among the metal cations [69].

The effects of ion concentration on protein-ion binding and intermolecular interactions, and consequently protein phase behavior, vary depending on the concentration range. (1) At very low ion concentrations, both charge screening and ion binding are generally nonspecific and impact protein electrostatic interactions, with saturation occurring at approximately 1 mol% [39]. (2) In the medium and high ion concentration range (above 1 mol%), most charges on proteins are effectively screened, resulting in reduced electrostatic interactions. Specific ion effects in this range are related to specific ion binding and protein hydration [39,63,70]. Our observations revealed that the chaotropic nitrate anion can bind to the protein surface, promoting aggregation and crystallization at 1 mol%. The increase in lysozyme solubility in 1–20 mol% EAN can be attributed to reduced intermolecular protein interactions, which is associated with indirect water-mediated effects, where ions compete for interfacial water in the transition and bulk layers. However, by the crystallographic structures, we only observed saturated ion binding of nitrate and formate from 1 mol% to 5 or 17 mol % in the hydration layer. (3) In the presence of hydrated ions, which have limited free water, the specific ion effects involve factors such as ion size, ion hydration, ion dissociation and pairing, and surface tension effects [54]. For instance, the large weakly hydrated thiocyanate ion can bind strongly to positive charges on proteins and nonpolar surfaces through surface tension effects [71]. The interplay between attractive intermolecular interactions, particularly nonelectrostatic dispersion forces, and surface tension contributes to the overall process of protein aggregation and denaturation [17]. It is important to note that the ion concentration can significantly affect the pH of IL solutions, which must be considered when using ILs as solvents [72]. Other theories should also be taken into consideration. (a) The preferential interaction theory explains that certain solutes have a higher affinity for specific components of the solvent compared to other solutes [73,74]. Kosmotropic anions, for example, are excluded from the protein surface, leading to preferential binding of water, increased surface tension, and reduced protein solubility. Conversely, chaotropic anions preferentially bind to the surface, resulting in preferential exclusion of water and increased protein solubility. (b) Factors such as solvation, the law of matching water affinities, polarizability, ion size, shape and hydrophobicity and Viscosity *B*-coefficients should be considered [70]. (c) The ion pair dissociation in aqueous solution can be complicated yet critical, as ions or ion pairs can interact with proteins directly or indirectly through mediation by water molecules [64]. In this study, the contact ion pair

interactions of EtAF with protein surfaces indicated that ion hydration in the bulk phase mediated the interactions. Most ILs exhibit lower degrees of dissociation (low ionicity), while EtAF and EAF are much less dissociated than most ILs [75]. On the other hand, conventional salts generally completely dissociate in water [64]. While the dissociated anions have a dominant effect for ILs, the ion pair and its dissociation can also have a destabilizing effect, which explains the loss of activity observed in EAF compared to EAN, EtAN, and EtAF. Overall, protein-water interfacial tension, excluded volume, ion pairs, and specific ion binding at the protein surface all play important roles in the complex behavior of proteins in solution.

3. Conclusions

We conducted an in-depth investigation of the effects of ILs on the behaviour and structure of the model protein hen egg white lysozyme, which involved a comprehensive analysis of the solubility, activity, size, shape, structure, and ion-protein binding of the protein with a focus on using two ILs, ethylammonium nitrate (EAN) and ethanolammonium formate (EtAF). Importantly, we probe the specific ion-binding at the protein interface at the molecular level and emphasize the effect of specific ion binding of ILs on the modulation of protein properties. Results show that the protein in EAN solutions had high solubility, but low enzyme activity and larger size changes, unlike EtAF, in both low and high concentrations. We observed more size and shape changes, elongated species, and irreversible aggregates in neat EAN than in neat EtAF. More anion binding sites of nitrate than formate, and an ion pair of EtAF were identified based on seven crystal structures with ILs present. A comparison of ion binding from a wide range of PDB structures in the presence of other anions revealed that ions, particularly anions, had direct electrostatic interactions with the positively charged side chains (especially R) and hydrogen bonding with polar residues (K, S and N) and aromatic residue (W for nitrate). It is highlighted that the specific ion binding on the protein observed in crystallographic structures is in the solvation layer, and it can induce more flexible loop regions in lysozyme. It should be noted that the ion binding in the solution phase can be more complex and dynamic. Interestingly, the ion binding in the solvation layer were saturated at 1 or 5 mol% ILs, with EAN having more ion binding sites than EtAF, which explains why EAN induced more lysozyme activity loss and larger size change at 1 mol%. However, the protein behaviour depends on the net effect of nonspecific intermolecular interactions and specific ion binding. There are a few conserved specific ion binding sites, which are reported for the first time in this work. Notably, the ion binding is clearly related to specific ion effects. The chaotropic nitrate anion acts to solubilize proteins and interacts more with proteins, compared to the kosmotropic formate anion which salts out proteins, but tends to reduce protein denaturation and interacts less with proteins. This finding is similar to the previously reported effect of salts with common anions [52,62,71,76] and metal ions [40,69,76], but here more specific ion binding was observed and higher ion concentrations were studied. Our study highlights the importance of combining phase behaviour determination, enzyme activity assays, and structural and ion binding analysis to gain a comprehensive understanding of the role of ILs, and their constituent ions, on proteins. We also show that the ion binding effect can slightly vary with the amino acid composition and pI of the proteins, and hence an in-depth, atom-by-atom inspection of ion binding for not only metal ions and common anions but also a broader range of ions and proteins, will benefit protein structure–property-based development and research, especially when designing solvents for protein stabilization and crystallization, controlling phase behaviour, biochemical processes, and investigating the biological function of proteins including protein aggregation-related disease. Overall, our findings provide further confirmation that understanding the interfacial behaviour of proteins in ILs is critical for optimizing their use in various applications.

4. Experimental section

4.1. Materials: Ethylamine (70% in H_2O), ethanolamine (99%), *n*-butylamine (99.5%), hexylamine (99%), nitric acid (70%), formic acid (≥98%), and lysozyme from chicken egg white powder (E.C. 3.2.1.17) were obtained commercially from Sigma Aldrich and were all used without further purification.

4.2. IL preparation The ILs were synthesized as reported previously [4,26]. In brief, the ILs were synthesized by neutralizing equimolar amounts of the corresponding acid and base at <5 °C. Excess water was removed under reduced pressure using a rotary evaporator followed by a freeze dryer. The water content of the ILs was measured using a Karl Fisher coulometer (Mettler Toledo DL39). The water content of all ILs was below 0.5 wt% after drying. The purity of ILs was confirmed by NMR. For aqueous ILs, a specified amount of the ILs were gravimetrically mixed with MilliQ water to reach the required concentration (Table S1). The pH of the aqueous IL solutions (1–17 mol%) was measured using a pH meter (Mettler Toledo) and then adjusted to a pH of 8 ± 0.2 by titrating with 2 M Tris [72]. The apparent pH of hydrated and neat ILs (greater than 17 mol%) was estimated by measuring the pH of their diluted aqueous solutions (~1 mol% or 10 wt%).

A Tris buffer (100 mM, pH 8) was used in all tests, unless otherwise stated. Lysozyme stock solutions were prepared by dissolving corresponding amount of lysozyme lyophilized powder in Tris buffer. Portions of this stock solution was added to the IL-water mixtures to obtain the final protein concentration for each test.

4.3. Phase diagram: Crystallization screening of lysozyme was performed at various concentrations of EAN and EtAF, and lysozyme concentrations, using the microbatch method. The solutions were prepared as follows. 100 μL of each IL solution was mixed with a specified amount of lysozyme powder in a vial. From this, one drop was added to the reservoir of a 96-well plate. The solutions were maintained at 20 °C, while the imaging of the protein crystals/aggregates in plates was carried out after 1 day using an Olympus IMT-2 microscope. Four possible phase states were classified from visual observations: soluble (clear solution), crystalized, precipitated (crystallization with precipitation), and insoluble (precipitation only), and these were used to construct phase diagrams. In highly concentrated lysozyme solutions, the gelation with insoluble protein powder was noted, while the edge of droplets was examined.

Solubility curves were determined by measuring the protein concentration in the supernatant of prepared lysozyme samples using the protein A280 method. After 2 h of incubating of lysozyme in saturated IL solutions, the samples were centrifuged, and 1 μL taken from the supernatant and analyzed using a NanoDrop 2000c spectrophotometer. The mass extinction coefficient of lysozyme is 2.64 mL mg^{-1} cm^{-1} at 280 nm.

4.4. Activity assay: The lysozyme activity was assayed based on turbidity change during the hydrolysis of 1,4-β-linkages in the cell wall of suspended *Micrococcus lysodeikticusce* cells using a Perkin Elmer EnSight Multimode Plate Reader. Cell suspensions was added into buffer or IL-water mixtures with a final cell concentration of 0.3% (w/v) and an initial absorbance of ~ 1.0 ± 0.1 at 450 nm at 20 °C. Lysozyme solution (5 mg/mL, 100 μL) in Tris buffer was added to the cell suspension, to have a final concentration of 0.1 mg/ml. The absorbance was then measured at 450 nm as a function of time. Control solutions of the cell suspension and IL without lysozyme produced a constant absorption signal. The relative activity was calculated based on the turbidity change in the IL solutions relative to the Tris buffer. Statistical analysis of relative activity was performed using the Student's *t*-test ($P < 0.05$).

4.5. SAXS: SAXS experiments were carried out at the SAXS/WAXS beamline at the Australian Synchrotron, Melbourne, Australia. The SAXS data were recorded on a Pilatus2-1 M silicon photon counting detector with an incident beam of wavelength λ = 1.033 Å (12.0 keV) and typical flux of around 10^{13} photons/s. The sample to detector distance was 2.4 m, with a *q*-range 0.005 to 0.55 $Å^{-1}$ as described

previously [24]. Lysozyme-IL samples (5 mg/mL, 100 μL) were loaded into the 96-well plate used for the automated sampling with a capillary and were equilibrated for about 10 h before measurement. Ten successive frames of 1 s exposure were collected for each sample and buffer and these were then averaged before further data processing. The SEC-SAXS setup was used with size-exclusion column GE Healthcare® Superdex S200 5 × 150 and high-performance liquid chromatography (HPLC, Agilent 1260). In each measurement, HPLC column was equilibrated with buffer for ~ 30 min, and then lysozyme-ILs samples (5 mg/mL, 50 μL) were injected with a flow rate of 0.40 mL/min. The UV absorbance at 280 nm and SAXS patterns were continuously acquired for 15 min. For the study of neat IL-treated lysozyme in, 5 mg/mL lysozyme was incubated in neat EAN or EtAF for 1 day and then ran through SEC-SAXS. To identified the space group of lysozyme crystals, the crystals were prepared with 20 mg/mL lysozyme and ran through plate transmission mode of SAXS[24].

Scatterbrain 2.82 was used for averaging and solvent subtraction of the SAXS data, and the ATSAS software package was used for SAXS data analysis [49]. Specifically, SAXS patterns are presented as the average of the measurements after accurate blank subtraction of the corresponding solvent [22]. The R_g for lysozyme was calculated using the Guinier approximation (where $qR_g < 1.3$ Å) through the ATSAS package. Kratky plots were plotted as q^2I against q, where q is the scattering vector, and I the scattering intensity. The distance distribution function $P(r)$ and the maximum diameter (D_{max}) were obtained using the ATSAS software, refering to the radius at which $p(r)$ approaches to zero. The patterns are presented with offset for comparison in the figures. CRYSOL was used to compare experimental SAXS scattering with the model scattering of lysozyme crystal structure PDB ID 7JMU [26]. Subsequently, SREFLEX was used for refinement and normal mode analysis from the initial structure 7JMU [49], and the best refined models in different ILs were selected based on the discrepancies χ^2 value. GASBOR program was used for *ab initio* constructing an ensemble of 90 dummy residues equivalent to the molecular mass of the lysozyme. Open-source PyMOL v. 1.8.4.0 (https://pymol.org/) was used to visually analyze and generate figures. The surface electrostatic representation was prepared using APBS [77]. Crystal phases were identified by visual comparison with known PDB structures.

4.6. Crystallography: For the crystallography experiment, a stock solution of 200 mg/mL lysozyme in Tris buffer was prepared and diluted 10-fold in IL-water mixtures (pH 8), resulting in a final concentration of 20 mg/mL. The crystals were prepared in 5 mol% EAN (ca. 20 wt%), 1 mol% EtAN and BAN (ca. 6 wt%) using microbatch method, and in 5, 7 and 17 mol% (ca. 20, 30 and 50 wt%, respectively) using vapor diffusion method. The lysozyme solutions were crystallized and kept for 1 week to obtain large crystals. A routine crystallography experiment was carried out. One crystal was isolated from the crystal solution and transferred to a cryo-protectant (Paratone 8277, Hampton Research). The crystal was immediately flash-frozen in liquid nitrogen and mounted on the MX2 (for EAN/EtAN/BAN structures) or MX1 (for EtAF structures) macromolecular beamline at the Australian Synchrotron. Data collection was carried out at 100 K. X-ray diffraction patterns were collected using a Dectris Eiger 16 M detector for MX2 and a Dectris Eiger2 9 M detector for MX1 [78]. Data reduction and integration were performed using XDS [79]. Merging, indexing and scaling was done using Aimless and the CCP4 suite [80], and 5% of the reflections were used for the R_{free} calculations. Phaser was used to phase the model using the molecular replacement approach with 1dpw used as the search model [81]. Iterative cycles of model building and refinement were performed with Coot [82] and Phenix v1.8 [83], respectively. Data collection and refinement statistics can be found in Table 1. The protein isoelectric point (pI) was calculated by Compute PI/MW tool.

CRediT authorship contribution statement

Qi Han: Conceptualization, Methodology, Investigation, Formal analysis, Writing – original draft, Writing – review & editing, Visualization. **Yuyu Su:** Validation, Writing – review & editing. **Kate M. Smith:** Resources, Writing – review & editing. **Jack Binns:** Validation, Writing – review & editing. **Calum J. Drummond:** Resources, Writing – review & editing, Supervision, Project administration. **Connie Darmanin:** Methodology, Investigation, Formal analysis, Validation, Writing – review & editing. **Tamar L. Greaves:** Methodology, Validation, Writing – review & editing, Supervision, Project administration.

Declaration of Competing Interest

The authors declare that they have no known competing financial interests or personal relationships that could have appeared to influence the work reported in this paper.

Data availability

Data will be made available on request.

Acknowledgment

The authors acknowledge funding support from the Australian Research Council under its Discovery grant Scheme for this work (DP230101712). The authors also acknowledge the use of the MX1, MX2 and SAXS/WAXS beamlines at the Australian Synchrotron, Melbourne, Australia.

Appendix A. Supplementary material

Supplementary data to this article can be found online at https://doi.org/10.1016/j.jcis.2023.07.045.

References

[1] T. Welton, Room-temperature ionic liquids. Solvents for synthesis and catalysis, Chem Rev 99 (8) (1999) 2071–2083.
[2] T.L. Greaves, C.J. Drummond, Protic ionic liquids: properties and applications, Chem Rev 108 (1) (2008) 206–237.
[3] D.R. MacFarlane, M. Kar, J.M. Pringle, Fundamentals of Ionic Liquids: From Chemistry to Applications, John Wiley & Sons, 2017.
[4] M. Yoshizawa, W. Xu, C.A. Angell, Ionic Liquids by Proton Transfer: Vapor Pressure, Conductivity, and the Relevance of ΔpKa from Aqueous Solutions, J Am Chem Soc 125 (50) (2003) 15411–15419.
[5] F.A. e Silva, J.F.B. Pereira, K.A. Kurnia, S.P.M. Ventura, A.M.S. Silva, R.D. Rogers, J.A.P. Coutinho, M.G. Freire, Temperature dependency of aqueous biphasic systems: an alternative approach for exploring the differences between Coulombic-dominated salts and ionic liquids, Chem Commun 53(53) (2017) 7298-7301.
[6] D.R. MacFarlane, A.L. Chong, M. Forsyth, M. Kar, R. Vijayaraghavan, A. Somers, J. M. Pringle, New dimensions in salt–solvent mixtures: a 4th evolution of ionic liquids, Faraday Discuss 206 (2018) 9–28.
[7] Y. Kohno, H. Ohno, Ionic liquid/water mixtures: from hostility to conciliation, Chem Commun 48 (57) (2012) 7119–7130.
[8] Q. Han, X. Wang, N. Bynre, Utilizing water activity as a simple measure to understand hydrophobicity in ionic liquids, Front Chem 7 (2019) 112.
[9] T.L. Greaves, C.J. Drummond, Protic Ionic Liquids: Evolving Structure-Property Relationships and Expanding Applications, Chem Rev 115 (20) (2015) 11379–11448.
[10] J.Q. Lai, Z. Li, Y.H. Lu, Z. Yang, Specific ion effects of ionic liquids on enzyme activity and stability, Green Chem 13 (7) (2011) 1860–1868.
[11] F. van Rantwijk, R.A. Sheldon, Biocatalysis in ionic liquids, Chem Rev 107 (6) (2007) 2757–2785.
[12] Y. Zhang, P.S. Cremer, Chemistry of Hofmeister anions and osmolytes, Ann Rev Phys Chem 61 (2010) 63–83.
[13] K.P. Gregory, G.R. Elliott, H. Robertson, A. Kumar, E.J. Wanless, G.B. Webber, V.S. J. Craig, G.G. Andersson, A.J. Page, Understanding specific ion effects and the Hofmeister series, Phys Chem Chem Phys 24 (21) (2022) 12682–12718.
[14] H. Weingartner, C. Cabrele, C. Herrmann, How ionic liquids can help to stabilize native proteins, Phys Chem Chem Phys 14 (2) (2012) 415–426.
[15] H. Zhao, Protein stabilization and enzyme activation in ionic liquids: specific ion effects, J Chem Technol Biot 91 (1) (2016) 25–50.
[16] L.O. Narhi, J. Schmit, K. Bechtold-Peters, D. Sharma, Classification of protein aggregates, J Pharm Sci-US 101 (2) (2012) 493–498.
[17] Q. Han, S. Brown, C.J. Drummond, T.L. Greaves, Protein aggregation and crystallization with ionic liquids: Insights into the influence of solvent properties, J Colloid Interf Sci 608 (2022) 1173–1190.

[18] N. Byrne, L.M. Wang, J.P. Belieres, C.A. Angell, Reversible folding-unfolding, aggregation protection, and multi-year stabilization, in high concentration protein solutions, using ionic liquids, Chem Commun 26 (2007) 2714–2716.
[19] J.P. Mann, A. McCluskey, R. Atkin, Activity and thermal stability of lysozyme in alkylammonium formate ionic liquids-influence of cation modification, Green Chem 11 (6) (2009) 785–792.
[20] L. Bui-Le, C.J. Clarke, A. Bröhl, A.P. Brogan, J.A. Arpino, K.M. Polizzi, J.P. Hallett, Revealing the complexity of ionic liquid–protein interactions through a multi-technique investigation, Comm Chem 3 (1) (2020) 1–9.
[21] R.P. Rambo, J.A. Tainer, Super-resolution in solution X-ray scattering and its applications to structural systems biology, Ann Rev Biophys 42 (2013) 415–441.
[22] C.M. Jeffries, M.A. Graewert, C.E. Blanchet, D.B. Langley, A.E. Whitten, D. I. Svergun, Preparing monodisperse macromolecular samples for successful biological small-angle X-ray and neutron-scattering experiments, Nat Protoc 11 (11) (2016) 2122–2153.
[23] E.C. Wijaya, F. Separovic, C.J. Drummond, T.L. Greaves, Stability and activity of lysozyme in stoichiometric and non-stoichiometric protic ionic liquid (PIL)-water systems, J Chem Phys 148 (19) (2018), 193838.
[24] Q. Han, J. Binns, J. Zhai, X. Guo, T.M. Ryan, C.J. Drummond, T.L. Greaves, Insights on lysozyme aggregation in protic ionic liquid solvents by using small angle X-ray scattering and high throughput screening, J Mol Liq 345 (2022), 117816.
[25] Q. Han, M. El Mohamad, S. Brown, J. Zhai, C.J. Rosado, Y. Shen, E.W. Blanch, C. J. Drummond, T.L. Greaves, Small angle X-ray scattering investigation of ionic liquid effect on the aggregation behavior of globular proteins, J Colloid Interf Sci 648 (2023) 376–388.
[26] Q. Han, K.M. Smith, C. Darmanin, T.M. Ryan, C.J. Drummond, T.L. Greaves, Lysozyme conformational changes with ionic liquids: Spectroscopic, small angle x-ray scattering and crystallographic study, J Colloid Interf Sci 585 (2021) 433–443.
[27] Q. Han, T.M. Ryan, C.J. Rosado, C.J. Drummond, T.L. Greaves, Effect of ionic liquids on the fluorescence properties and aggregation of superfolder green fluorescence protein, J Colloid Interf Sci 591 (2021) 96–105.
[28] J.A. Garlitz, C.A. Summers, R.A. Flowers, G.E. Borgstahl, Ethylammonium nitrate: a protein crystallization reagent, Acta Crystallogr D Biol Crystallogr 55 (12) (1999) 2037–2038.
[29] R.A. Judge, S. Takahashi, K.L. Longenecker, E.H. Fry, C. Abad-Zapatero, M.L. Chiu, The effect of ionic liquids on protein crystallization and X-ray diffraction resolution, Crys Growth Des 9 (8) (2009) 3463–3469.
[30] D.F. Kennedy, C.J. Drummond, T.S. Peat, J. Newman, Evaluating protic ionic liquids as protein crystallization additives, Cryst Growth Des 11 (5) (2011) 1777–1785.
[31] B.D. Belviso, R. Caliandro, S.M. Salehi, G. Di Profio, R. Caliandro, Protein crystallization in ionic-liquid hydrogel composite membranes, Crystals 9 (5) (2019) 253.
[32] C.L. Tarver, Q. Yuan, M.L. Pusey, Ionic Liquids as Protein Crystallization Additives, Crystals 11 (10) (2021) 1166.
[33] M. Kowacz, A. Mukhopadhyay, A.L. Carvalho, J.M.S.S. Esperança, M.J. Romão, L. P.N. Rebelo, Hofmeister effects of ionic liquids in protein crystallization: Direct and water-mediated interactions, Crystengcomm 14 (15) (2012) 4912–4921.
[34] P. Ganguly, J. Polák, N.F.A. van der Vegt, J. Heyda, J.-E. Shea, Protein stability in TMAO and mixed urea–TMAO solutions, J Phys Chem B 124 (29) (2020) 6181–6197.
[35] M. Reslan, V. Kayser, Ionic liquids as biocompatible stabilizers of proteins, Biophys Rev 10 (3) (2018) 781–793.
[36] A. Schindl, M.L. Hagen, S. Muzammal, H.A.D. Gunasekera, A.K. Croft, Proteins in ionic liquids: Reactions, applications, and futures, Front Chem 7 (2019) 347.
[37] R. Ferraz, A.T. Silva, C. Teixeira, E.F.M.F. Marques, C. Prudêncio, P. Gomes, Surfing the third wave of ionic liquids: a brief review on the role of surface-active ionic liquids in drug development and delivery, Chemmedchem 16 (2021) 2604–2611.
[38] Z. Li, Q. Han, K. Wang, S. Song, Y. Xue, X. Ji, J. Zhai, Y. Huang, S. Zhang, Ionic liquids as a tunable solvent and modifier for biocatalysis, Catal Rev Sci Eng (2022) 1–47.
[39] Y. Zhang, P.S. Cremer, The inverse and direct Hofmeister series for lysozyme, Proc Natl Acad Sci USA 106 (36) (2009) 15249–15253.
[40] T. Dudev, C. Lim, Principles governing Mg, Ca, and Zn binding and selectivity in proteins, Chem Rev 103 (3) (2003) 773–788.
[41] E.C. Wijaya, F. Separovic, C.J. Drummond, T.L. Greaves, Activity and conformation of lysozyme in molecular solvents, protic ionic liquids (PILs) and salt–water systems, Phys Chem Chem Phys 18 (37) (2016) 25926–25936.
[42] R. Kanzaki, H. Kodamatani, T. Tomiyasu, H. Watanabe, Y. Umebayashi, A pH Scale for the Protic Ionic Liquid Ethylammonium Nitrate, Angew Chem Int Ed 128 (21) (2016) 6374–6377.
[43] D.R. MacFarlane, J.M. Pringle, K.M. Johansson, S.A. Forsyth, M. Forsyth, Lewis base ionic liquids, Chem Commun 18 (2006) 1905–1917.
[44] N. Byrne, C.A. Angell, The solubility of hen lysozyme in ethylammonium nitrate/H2O mixtures and a novel approach to protein crystallization, Molecules 15 (2) (2010) 793–803.
[45] N. Asherie, Protein crystallization and phase diagrams, Methods 34 (3) (2004) 266–272.
[46] D. Erdemir, A.Y. Lee, A.S. Myerson, Nucleation of crystals from solution: classical and two-step models, Acc Chem Res 42 (5) (2009) 621–629.
[47] Q. Han, H.C. Broomhall, N. Vieira Veríssimo, T.M. Ryan, C.J. Drummond, J.F. B. Pereira, T.L. Greaves, Protic Ionic Liquid Cation Alkyl Chain Length Effect on Lysozyme Structure, Molecules 27 (3) (2022) 984.
[48] D. Svergun, S. Richard, M. Koch, Z. Sayers, S. Kuprin, G. Zaccai, Protein hydration in solution: experimental observation by x-ray and neutron scattering, Proc Natl Acad Sci USA 95 (5) (1998) 2267–2272.
[49] A. Panjkovich, D.I. Svergun, Deciphering conformational transitions of proteins by small angle X-ray scattering and normal mode analysis, Phys Chem Chem Phys 18 (8) (2016) 5707–5719.
[50] D.I. Svergun, M.V. Petoukhov, M.H.J. Koch, Determination of domain structure of proteins from X-ray solution scattering, Biophys J 80 (6) (2001) 2946–2953.
[51] S. Bellmaine, A. Schnellbaecher, A. Zimmer, Reactivity and degradation products of tryptophan in solution and proteins, Free Radic Biol Med 160 (2020) 696–718.
[52] M. Plaza-Garrido, M.C. Salinas-Garcia, A. Camara-Artigas, Orthorhombic lysozyme crystallization at acidic pH values driven by phosphate binding, Acta Crystallogr D Struct Biol 74 (5) (2018) 480–489.
[53] E.P. O'Brien, R.I. Dima, B. Brooks, D. Thirumalai, Interactions between hydrophobic and ionic solutes in aqueous guanidinium chloride and urea solutions: lessons for protein denaturation mechanism, J Am Chem Soc 129 (23) (2007) 7346–7353.
[54] H.-X. Zhou, X. Pang, Electrostatic interactions in protein structure, folding, binding, and condensation, Chem Rev 118 (4) (2018) 1691–1741.
[55] M.S. Weiss, G.J. Palm, R. Hilgenfeld, Crystallization, structure solution and refinement of hen egg-white lysozyme at pH 8.0 in the presence of MPD, Acta Crystallogr D Biological Crystallogr 56 (8) (2000) 952–958.
[56] C. Sauter, F. Otálora, J.A. Gavira, O. Vidal, R. Giegé, J.M. García-Ruiz, Structure of tetragonal hen egg-white lysozyme at 0.94 Å from crystals grown by the counter-diffusion method, Acta Crystallogr D Biol Crystallogr 57 (8) (2001) 1119–1126.
[57] M. Sugahara, T. Nakane, T. Masuda, M. Suzuki, S. Inoue, C. Song, R. Tanaka, T. Nakatsu, E. Mizohata, F. Yumoto, Hydroxyethyl cellulose matrix applied to serial crystallography, Sci Rep-UK 7 (1) (2017) 703.
[58] L. Steinrauf, Structures of monoclinic lysozyme iodide at 1.6 Å and of triclinic lysozyme nitrate at 1.1 Å, J Acta Crystallographica D Biol Crystallogr 54 (5) (1998) 767–779.
[59] J. Wang, M. Dauter, R. Alkire, A. Joachimiak, Z. Dauter, Triclinic lysozyme at 0.65 Å resolution, Acta Crystallogr D Biol Crystallogr 63 (12) (2007) 1254–1268.
[60] M. Kitahara, S. Fudo, T. Yoneda, M. Nukaga, T. Hoshino, Anisotropic distribution of ammonium sulfate ions in protein crystallization, Cryst Growth Des 19 (11) (2019) 6004–6010.
[61] T. Raskar, C.Y. Koh, S. Niebling, R.M. Kini, M.V. Hosur, X-ray crystallographic analysis of time-dependent binding of guanidine hydrochloride to HEWL: First steps during protein unfolding, Int J Biol Macromol 122 (2019) 903–913.
[62] M.C. Vaney, I. Broutin, P. Retailleau, A. Douangamath, S. Lafont, C. Hamiaux, T. Prangé, A. Ducruix, M. Riès-Kautt, Structural effects of monovalent anions on polymorphic lysozyme crystals, Acta Crystallogr D Biol Crystallogr 57 (7) (2001) 929–940.
[63] Y.R. Gokarn, R.M. Fesinmeyer, A. Saluja, V. Razinkov, S.F. Chase, T.M. Laue, D. N. Brems, Effective charge measurements reveal selective and preferential accumulation of anions, but not cations, at the protein surface in dilute salt solutions, Protein Sci 20 (3) (2011) 580–587.
[64] O. Nordness, J.F. Brennecke, Ion dissociation in ionic liquids and ionic liquid solutions, Chem Rev 120 (23) (2020) 12873–12902.
[65] K.D. Collins, Ions from the Hofmeister series and osmolytes: effects on proteins in solution and in the crystallization process, Methods 34 (3) (2004) 300–311.
[66] A.C. Dumetz, A.M. Snellinger-O'Brien, E.W. Kaler, A.M. Lenhoff, Patterns of protein–protein interactions in salt solutions and implications for protein crystallization, Protein Sci 16 (9) (2007) 1867–1877.
[67] R. Okajima, S. Hiraoka, T. Yamashita, Environmental Effects on Salt Bridge Stability in the Protein-Protein Interface: The Case of Hen Egg-White Lysozyme and Its Antibody, HyHEL-10, J Phys Chem B 125 (6) (2021) 1542–1549.
[68] L.M. Pegram, M.T. Record, Hofmeister salt effects on surface tension arise from partitioning of anions and cations between bulk water and the air− water interface, J Phys Chem B 111 (19) (2007) 5411–5417.
[69] H.I. Okur, J. Kherb, P.S. Cremer, Cations Bind Only Weakly to Amides in Aqueous Solutions, J Am Chem Soc 135 (13) (2013) 5062–5067.
[70] D. Roberts, R. Keeling, M. Tracka, C.F. van der Walle, S. Uddin, J. Warwicker, R. Curtis, Specific Ion and Buffer Effects on Protein-Protein Interactions of a Monoclonal Antibody, Mol Pharm 12 (1) (2015) 179–193.
[71] K.D. Collins, Why continuum electrostatics theories cannot explain biological structure, polyelectrolytes or ionic strength effects in ion–protein interactions, Biophys Chem 167 (2012) 43–59.
[72] Q. Han, X. Wang, N. Byrne, A Simple Approach to Achieve Self-Buffering Protic Ionic Liquid-Water Mixtures, ChemistrySelect 2 (15) (2017) 4294–4299.
[73] S.N. Timasheff, Protein hydration, thermodynamic binding, and preferential hydration, Biochemistry-US 41 (46) (2002) 13473–13482.
[74] S.N. Timasheff, Protein-solvent preferential interactions, protein hydration, and the modulation of biochemical reactions by solvent components, Proc Natl Acad Sci USA 99 (15) (2002) 9721–9726.
[75] B. Nuthakki, T.L. Greaves, I. Krodkiewska, A. Weerawardena, M.I. Burgar, R. J. Mulder, C.J. Drummond, Protic ionic liquids and ionicity, Aust J Chem 60 (1) (2007) 21–28.
[76] J.M. Fox, K. Kang, W. Sherman, A. Héroux, G.M. Sastry, M. Baghbanzadeh, M. R. Lockett, G.M. Whitesides, Interactions between Hofmeister Anions and the Binding Pocket of a Protein, J Am Chem Soc 137 (11) (2015) 3859–3866.
[77] E. Jurrus, D. Engel, K. Star, K. Monson, J. Brandi, L.E. Felberg, D.H. Brookes, L. Wilson, J. Chen, K. Liles, Improvements to the APBS biomolecular solvation software suite, Protein Sci 27 (1) (2018) 112–128.
[78] D. Aragao, J. Aishima, H. Cherukuvada, R. Clarken, M. Clift, N.P. Cowieson, D. J. Ericsson, C.L. Gee, S. Macedo, N. Mudie, MX2: a high-flux undulator microfocus

beamline serving both the chemical and macromolecular crystallography communities at the Australian Synchrotron, J Synchrotron Rad 25 (3) (2018) 885–891.
[79] W. Kabsch, Xds, Acta Crystallographica Section D: Biological Crystallography 66(2) (2010) 125-132.
[80] M.D. Winn, C.C. Ballard, K.D. Cowtan, E.J. Dodson, P. Emsley, P.R. Evans, R. M. Keegan, E.B. Krissinel, A.G. Leslie, A. McCoy, Overview of the CCP4 suite and current developments, Acta Crystallogr D Biol Crystallogr 67 (4) (2011) 235–242.
[81] A.J. McCoy, R.W. Grosse-Kunstleve, P.D. Adams, M.D. Winn, L.C. Storoni, R. J. Read, Phaser crystallographic software, J Appl Crystallogr 40 (4) (2007) 658–674.
[82] A. Casañal, B. Lohkamp, P. Emsley, Current developments in Coot for macromolecular model building of Electron Cryo-microscopy and Crystallographic Data, Protein Sci 29 (4) (2020) 1069–1078.
[83] D. Liebschner, P.V. Afonine, M.L. Baker, G. Bunkoczi, V.B. Chen, T.I. Croll, B. Hintze, L.-W. Hung, S. Jain, A.J. McCoy, N.W. Moriarty, R.D. Oeffner, B.K. Poon, M.G. Prisant, R.J. Read, J.S. Richardson, D.C. Richardson, M.D. Sammito, O. V. Sobolev, D.H. Stockwell, T.C. Terwilliger, A.G. Urzhumtsev, L.L. Videau, C. J. Williams, P.D. Adams, Macromolecular structure determination using X-rays, neutrons and electrons: recent developments in Phenix, Acta Crystallogr D Biol Crystallogr 75 (10) (2019) 861–877.